



**Development of Six-port Interferometer using
Substrate Integrated Waveguide Technique for
Radar-Based Sensor Application**

by

**Tan Gan Siang
(1640212037)**

A **thesis** submitted in **fulfillment** of the requirements for the degree of
Doctor of Philosophy

**School of Computer and Communication Engineering
UNIVERSITI MALAYSIA PERLIS**

2019

ACKNOWLEDGMENT

First, I would like to express my special gratitude to my main supervisor, Dr. Siti Zuraidah binti Ibrahim for giving me the opportunity to conduct this PhD research. I would like to thank her for her patience, encouragement and inspiration in providing me with invaluable advice and guidance throughout this research work. I would also like to thank my co-supervisor, Dr. Mohammad Shahrazel bin Razalli for his advice and support. I would like to thank my friend Sam Weng Yik for his advice and guidance throughout this research work. I would like to thank all the lecturers and postgraduate students at the faculty, who have helped in one way or another.

I would like to thank for the financial support on fabrication materials and publication by UniMAP under Fundamental Research Grant Scheme (FRGS 2015/1), FRGS/1/2015/TK04/UNIMAP/02/16 by the Ministry of Malaysia Education. I also like to thank USM Nibong Tebal School of Electrical and Electronic for the fabrication and measurement facilities and also Engineering Centre, UniMAP for the fabrication process.

Finally, I want to thank my mother, Lim Meng Su, my brother, Tan Gan Shen and my sisters, Tan Soo Wen and Tan Soo Fung, for their confidence in me, their encouragement and support throughout the duration of my studies.

TABLE OF CONTENTS

	PAGE
DECLARATION OF THESIS	i
TABLE OF CONTENTS	iii
LIST OF TABLES	vii
LIST OF FIGURES	viii
LIST OF ABBREVIATIONS	xiv
LIST OF SYMBOLS	xv
ABSTRAK	xvi
ABSTRACT	xvii
CHAPTER 1 INTRODUCTION	1
1.1 Research Background	1
1.2 Problem Statement	3
1.3 The Objectives of The Study	4
1.4 Research Scopes	5
1.5 Research Contribution	6
1.6 Thesis Outline	7
CHAPTER 2 LITERATURE REVIEW	9
2.1 Introduction	9
2.2 Radar-based Sensor Application	9
2.3 Six-port Interferometer	13
2.4 Substrate Integrated Waveguide	16

2.4.1	SIW Structure	17
2.4.2	Microstrip to SIW Transition	21
2.5	Six-port Main Components	24
2.5.1	SIW Power Divider	24
2.5.2	SIW Coupler	30
2.5.3	SIW Six-port	34
2.6	Summary	38
CHAPTER 3 METHODOLOGY		40
3.1	Introduction	40
3.2	Project Overview	40
3.3	Design Specification	41
3.3.1	Design Specification for SIW Power Dividers	42
3.3.2	Design Specification for SIW Hybrid Couplers	43
3.3.3	Design Specification for SIW Six-port	44
3.4	Flowchart	45
3.5	Design and Simulation	47
3.5.1	SIW Width and Via Holes Determination	48
3.5.2	Design and Configuration of SIW Power Dividers	50
3.5.2.1	Single Layer SIW Power Divider	51
3.5.2.2	Dual-layer SIW Power Divider	53
3.5.3	Design and Configuration of SIW Hybrid Coupler	56
3.5.4	Design and Configuration of SIW Six-port	58
3.5.5	Validation of The Design	61
3.5.6	Microstrip Line to SIW Transition	62
3.6	Fabrication	62
3.6.1	Fabrication Materials	62
3.6.2	Fabrication Process	63

3.6.3	Fabricated Prototypes	66
3.7	Measurement	68
3.7.1	Vector Network Analyzer	68
3.7.2	Measurement Process	69
3.8	Summary	72
CHAPTER 4 Results & Discussion		73
4.1	Introduction	73
4.2	Simulation Results of SIW Power Divider	73
4.2.1	Parametric Study on Dual-layer SIW Power Divider	74
4.2.1.1	Parametric Study on Slot	74
4.2.1.2	Parametric Study on the Top Substrate Layer	76
4.2.1.3	Parametric Study on the Top Substrate Layer Thickness	78
4.2.2	Simulation Results at X-band, Ku-band and K-band	80
4.3	Simulation Results of SIW Hybrid Coupler	86
4.3.1	Parametric Study on SIW Hybrid Coupler	87
4.3.2	Simulation Result of SIW Coupler at Ku-band and K-band	90
4.4	Simulation Results of SIW Six-port	93
4.4.1	Simulation Results of Single Layer SIW Six-port	93
4.4.2	Simulation Results of Single Layer and Dual-layer SIW Six-port at K-band	96
4.5	Measurement Results	101
4.5.1	Measurement Results of SIW Power Divider at X-band and Ku-band	102
4.5.2	Measurement Results of SIW Hybrid Coupler at Ku-band	105
4.5.3	Measurement Results of SIW Six-port Ku-band	107
4.6	Performance Comparison	112
4.6.1	SIW Power Divider with Previous SIW Wilkinson Power Divider	112
4.6.2	SIW Hybrid Coupler with Previous SIW Coupler	113

4.6.3	SIW Six-port with Previous SIW Six-port	114
4.7	Summary	115
CHAPTER 5 Conclusion		117
5.1	Conclusion	117
5.2	Future Work	119
REFERENCES		121
APPENDIX A RO4003C DATA SHEET		127
APPENDIX B SMA CONNECTOR DATA SHEET		128
APPENDIX C STANDARD RECTANGULAR WAVEGUIDE DATA		130
LIST OF PUBLICATION		131

LIST OF TABLES

		PAGE
Table 2.1	Standard Radar-Frequency Letter-Band Nomenclature (International Telecommunication Union, 2016)	13
Table 2.2	Comparison of the previous SIW power dividers at X-band	29
Table 2.3	Comparison of the previous SIW couplers	33
Table 2.4	Comparison of the previous SIW six-ports	38
Table 3.1	Specification of RO4003C	42
Table 3.2	Design specification of single layer SIW power dividers	43
Table 3.3	Design specification of dual-layer SIW power dividers	43
Table 3.4	Design specification of SIW hybrid couplers	44
Table 3.5	Design specification of SIW six-port	45
Table 4.1	Simulation results of the single layer and dual-layer SIW power dividers	84
Table 4.2	Comparison of the dual-layer SIW power divider with previous SIW power divider	113
Table 4.3	Comparison of the designed SIW hybrid coupler with previous SIW coupler	114
Table 4.4	Comparison of the single layer SIW six-port with previous SIW six-port	115

LIST OF FIGURES

	PAGE	
Figure 2.1	Optical technique detection in dusty environment (Vinci, Lindner, Barbon, Weigel, & Koelpin, 2012)	10
Figure 2.2	Radar technique detection in dusty environment (Vinci, Lindner, Barbon, Weigel, & Koelpin, 2012)	11
Figure 2.3	Six-port based DOA detection	14
Figure 2.4	Structure of Substrate Integrated Waveguide (Xu & Wu, 2005)	17
Figure 2.5	Cutoff frequencies of the TE ₁₀ -like and TE ₂₀ -like modes of the straight pattern SIRW vs. width W for various via diameters D (Cassivi et.al, 2002)	18
Figure 2.6	Dominant mode electric profiles: (a) rectangular waveguide; (b) microstrip line (Pozar, 2005)	22
Figure 2.7	Taper transition of microstrip line to SIW	23
Figure 2.8	Schematic of power divider.	25
Figure 2.9	T-junction configuration (Kazemi, Sadeghzadeh, & Fathy, 2012)	26
Figure 2.10	HMSIW with resistor chip (Kim, Byun, & Lee, 2010)	26
Figure 2.11	SIW power divider with butterfly slots (Chen, Zhang, & Yu, 2013)	27
Figure 2.12	Ring shaped SIW power divider with resistor (Jerafi, Hammou, Wu, & Tatu, 2014)	28

Figure 2.13	SIW coupler with narrow aperture and additional via holes (Tavakoli & Mallahzadeh, 2018)	31
Figure 2.14	SIW with U symmetrical configuration (Nouri, Feham, Damou, & Bouazza, 2014)	31
Figure 2.15	SIW coupler with additional via holes (Nasri, Zairi, & Gharsallah, 2016)	32
Figure 2.16	SIW six-port with dual-layer configuration (Kramer, Djerafi, & Wu, 2012)	35
Figure 2.17	HMSIW six-port with four couplers (Chen, et al., 2012)	36
Figure 2.18	SIW six-ports with four coupler (Lakhdhar, Harabi, & Gharsallah, 2015)	36
Figure 2.19	SIW six-port with one power divider and three couplers (Jafari, Moradi, Shirazi, & Mirzavand, 2017)	37
Figure 3.1	Topology of six-port	41
Figure 3.2	Flowchart of the development of the SIW six-port.	47
Figure 3.3	Single layer SIW power divider	51
Figure 3.4	Flow chart of the development of the single layer SIW power divider.	52
Figure 3.5	Dual-layer SIW power divider configuration (a) layer view (b) top substrate layer (c) base substrate layer	54
Figure 3.6	Flowchart of the development of the dual-layer SIW power divider	55
Figure 3.7	SIW hybrid coupler (a) layer structure (b) top view	56
Figure 3.8	Flowchart of the simulation process of the SIW hybrid coupler.	58

Figure 3.9	Single layer SIW six-port configuration (a) layer structure (b) substrate layer	59
Figure 3.10	Dual-layer SIW six-port configuration (a) layers structure (b) base layer and top layer structures	60
Figure 3.11	Flowchart of the development of the SIW six-port.	61
Figure 3.12	A flow diagram process of the fabrication process on first type SIW prototype	64
Figure 3.13	A flow diagram process of the fabrication process on second type SIW prototypes	65
Figure 3.14	Fabricated dual-layer SIW power divider (a) front view (b) back view	66
Figure 3.15	Fabricated SIW single layer power divider (a) front view (b) back view	67
Figure 3.16	Fabricated SIW hybrid coupler (a) front view (b) back view	67
Figure 3.17	Fabricated SIW six-port (a) front view (b) back view	68
Figure 3.18	Block diagram of the S-parameter measurements performed on power divider.	70
Figure 3.19	Block diagram of the S-parameter measurements performed on the coupler	71
Figure 3.20	Block diagram of the S-parameter measurements performed on six-port	72
Figure 4.1	Parameters value of the dual-layer SIW power divider for parametric study on slot	75
Figure 4.2	Simulation results of parametric study of S_{32} (a) slot width, S_w and (b) slot length, S_l	76

Figure 4.3	Parameters value of the dual-layer SIW power divider for parametric study on the top layer	77
Figure 4.4	Simulation results of parametric study of S_{32} (a) different copper width, C_w and (b) different copper length, C_l	78
Figure 4.5	Parameters value of the dual-layer SIW power divider for parametric study on top substrate thickness	79
Figure 4.6	Simulation results of parametric study of S_{32} on different top substrate layer thickness	80
Figure 4.7	Dimension of single-layer SIW power divider at (a) X-band and (b) K-band in mm.	81
Figure 4.8	Dimension of dual-layer SIW power divider at X-band in mm.	81
Figure 4.9	Dimension of dual-layer SIW power divider at K-band in mm.	81
Figure 4.10	Simulation of S-parameters results of (a) S_{11} , S_{21} , and S_{31} (b) S_{22} , S_{33} , and S_{32} single layer and dual-layer SIW power divider at X-band	82
Figure 4.11	Simulation of S-parameters results of (a) S_{11} , S_{21} , and S_{31} (b) S_{22} , S_{33} , and S_{32} single layer and dual-layer SIW power divider at K-band	83
Figure 4.12	Simulation results of E-field of the (a) Y-junction and (b) dual-layer SIW power divider	85
Figure 4.13	Dimension of single layer SIW power divider at Ku-band in mm	85
Figure 4.14	Simulation of S-parameters results of single layer SIW power divider at Ku-band	86

Figure 4.15	Parameters value of the SIW hybrid coupler for parametric study	87
Figure 4.16	Simulation results of parametric study of l_p (a) S_{11} and S_{41} (b) S_{21} and S_{31} at K-band	88
Figure 4.17	Simulation results of parametric study of c_a (a) S_{11} and S_{41} (b) S_{21} and S_{31} at K-band	89
Figure 4.18	Dimension of SIW hybrid coupler at Ku-band in mm.	90
Figure 4.19	Simulation S-parameter of SIW hybrid coupler at Ku-band	91
Figure 4.20	Dimension of SIW hybrid coupler at K-band in mm	92
Figure 4.21	Simulation results of S-parameter of SIW hybrid coupler at K-band	92
Figure 4.22	Designed single layer SIW six-port configuration at Ku-band	94
Figure 4.23	Simulation results of SIW six-port at Ku-band (a) S_{11} , S_{31} , S_{41} , S_{51} and S_{61} (b) S_{21} , S_{32} , S_{42} , S_{52} and S_{62} (c) Phase differences	95
Figure 4.24	Designed single layer SIW six-port configuration at K-band	96
Figure 4.25	Designed dual-layer SIW six-port configuration at Ku-band	97
Figure 4.26	Simulation results of single layer SIW six-port at K-band (a) S_{11} , S_{31} , S_{41} , S_{51} and S_{61} (b) S_{21} , S_{32} , S_{42} , S_{52} and S_{62} (c) phase differences	98
Figure 4.27	Simulation results of dual-layer SIW six-port at K-band (a) S_{11} , S_{31} , S_{41} , S_{51} and S_{61} (b) S_{21} , S_{32} , S_{42} , S_{52} and S_{62} (c) phase differences	100
Figure 4.28	Comparison of simulation results of S_{43} and S_{65} between single layer and dual-layer SIW six-port at K-band	101

Figure 4.29	Measurement results of dual-layer SIW power divider (a) S_{11} , S_{21} , and S_{31} (b) S_{32} at X-band	103
Figure 4.30	Measurement results of single layer SIW power divider (a) S_{11} and S_{32} (b) S_{21} , and S_{31} at Ku-band	105
Figure 4.31	Measurement results of SIW hybrid coupler (a) S_{11} and S_{41} (b) S_{21} , and S_{31} at Ku-band	107
Figure 4.32	Measurement results of SIW six-port at Ku-band (a) S_{11} and S_{21} (b) S_{31} , and S_{41} (c) S_{51} , and S_{61} (d) S_{32} , and S_{42} (e) S_{52} , and S_{62}	110
Figure 4.33	Measurement and Simulation phase different (a) S_{41} - S_{31} and S_{42} - S_{32} (b) S_{61} - S_{51} and S_{62} - S_{52} at Ku-band	111

LIST OF ABBREVIATIONS

ACC	Adaptive Cruise Control
AEB	Autonomous Emergency Braking
BI-RME	Boundary Integral-Resonant Mode Expansion
CNC	Computer Numerical Control
CPW	Coplanar Waveguide
DGS	Defective Ground Structure
DOA	Direction-of-Arrival
E-SIW	Empty Substrate Integrated Waveguide
GCPW	Grounded Coplanar Waveguide
HMSIW	Half-mode Substrate Integrated Waveguide
MBMR	Multi-beam Multi-range Radars
MMIC	Monolithic Microwave Integrated Circuits
PCB	Printed Circuit Board
PTH	Plated Through Hole
SIW	Substrate Integrated Waveguide
SMA	SubMiniature version A
TE	Transverse Electric
TEM	Transverse Electromagnetic Mode
VNA	Vector Network Analyzer

LIST OF SYMBOLS

Z_o	Characteristic Impedance (ohm)
ϵ_r	Relative Permittivity of Substrate
ϵ_{reff}	Effective Permittivity
h	Thickness of Substrate (mm)
$\tan \delta$	Tangent Loss
W_{eff}	Effective Width of SIW (mm)
p	Distance between via (mm)
d	Diameter of via (mm)
c	Velocity of light
W_m	Width of microstrip TL (mm)
W_t	Width of transition Taper (mm)
L_t	Length of transition Taper (mm)

@This item is protected by original copyright

Pembangunan Interferometer Enam-Liang Menggunakan Teknik Pandu Gelombang Substrat Bersepadu untuk Aplikasi Radar Berasaskan Penderia

ABSTRAK

Dalam kajian ini, penyelidikan ini menumpukan kepada pembangunan interferometer enam-liang menggunakan teknik Pandu Gelombang Substrat Bersepadu (SIW) di mana ia dapat berfungsi sebagai komponen di dalam radar berasaskan penderia. Menurut kerja-kerja kajian dulu yang dibentangkan dalam kesusasteraan terbuka, kebanyakan rekabentuk enam-liang SIW mempunyai liang tambahan yang tidak digunakan dan memerlukan beban penamat yang sepadan. Di samping itu, prestasi konvensional SIW enam-liang mengalami prestasi pengasingan yang rendah antara dua liang masukannya, disumbangkan oleh komponen pembahagi kuasa konvensional yang digunakan untuk membentuk enam-liang SIW. Salah satu kaedah yang dilaksanakan pada masa lalu untuk meningkatkan prestasi pengasingan adalah dengan menggunakan perintang pengasingan antara liang keluaran pembahagi kuasa tersebut. Walau bagaimanapun, cabaran timbul apabila frekuensi operasi meningkat, di mana saiz yang sesuai bagi perintang adalah sukar dicapai. Oleh itu, satu konfigurasi baru enam-liang SIW tanpa liang yang tidak digunakan dicadangkan dalam kajian ini. Untuk meningkatkan prestasi pengasingannya tanpa menggunakan perintang, pembahagi kuasa dwi lapisan baru dicadangkan dalam tesis ini. Semua simulasi yang direka menggunakan Studio Microwave CST dan fabrikasi dilakukan dengan menggunakan substrat Rogers 4003C dengan pemalar dielektrik sebanyak 3.38. Oleh kerana komponen utama enam-liang SIW adalah pembahagi kuasa dan penyambung hibrid, maka pengasingan pembahagi dan penyambung hibrid direka terlebih dahulu menggunakan teknik lapisan tunggal. Semua komponen direkabentuk pada jalur-Ku dan jalur-K, tetapi untuk demonstrasi prototaip, hanya reka bentuk di jalur-Ku direka dan diukur. Untuk pembahagi kuasa SIW dwi lapisan, rekabentuk disiasat pada jalur-X, jalur Ku dan jalur-K tetapi fabrikasi dan pengukuran dilakukan hanya pada jalur-X kerana cabaran fabrikasi penjajaran dan kewujudan jurang udara antara lapisan substrat. Penyambung SIW yang direka di jalur-Ku mempunyai lebar jalur kira-kira 31%. SIW enam-liang tanpa liang yang tidak digunakan dibentuk menggunakan satu lapisan pembahagi kuasa SIW dan penyambung hibrid SIW, yang saling terhubung dengan talian penghantaran. Ia berjaya direka pada frekuensi tengah 14.5 GHz dan mempunyai lebar jalur kira-kira 20%. Pembahagi kuasa dwi lapisan SIW direka pada 12 GHz dan mempunyai pengasingan tinggi kira-kira 43 dB pada 12.1 GHz. Dalam kerja masa depan, jalur lebar enam port SIW boleh ditingkatkan dengan memanjangkan panjang talian penghantaran pengasingan pembahagi SIW dan menambahkan tunggul terbuka untuk meningkatkan lebar jalur pembahagi kuasa SIW, yang seterusnya meningkatkan lebar jalur SIW enam-liang. Struktur pelbagai lapisan juga mempunyai potensi untuk mengurangkan dimensi terakhir SIW enam-liang. Untuk struktur dwi-lapisan, penyelidikan seterusnya boleh dilakukan pada SIW untuk peralihan talian slot untuk meningkatkan prestasi pengasingan.

Development of Six-port Interferometer using Substrate Integrated Waveguide Technique for Radar Based Sensor Application

ABSTRACT

In this work, the research is focused on the development of a six-port interferometer using Substrate Integrated Waveguide (SIW) technique where it can be worked as a component for the radar-based sensor. According to the past presented works in the open literature, most of the SIW six-port designs have an additional unused port and required a matched load termination. Besides, the performance of a conventional SIW six-port suffers from low isolation performance between its two input ports contributed by the conventional power divider component that is used to form the SIW six-port. One of the methods implemented in the past to improve the isolation performance is by introducing the isolation resistor between the output ports of the power divider. However, challenges arise when operating frequency increases as the appropriate size of the resistor are difficult to achieve. Therefore, a new configuration of the SIW six-port without unused port is proposed in this research. To improve its isolation performance without the use of a resistor, a new dual-layer power divider is proposed in this thesis. All the designed simulation is performed using CST Microwave Studio and the fabrication is done using Rogers 4003C substrate with a dielectric constant of 3.38. Since the key components of the SIW six-port are the power divider and hybrid couplers, hence the power divider and hybrid couplers are designed first using the single layer technique. All the components are designed at Ku-Band and K-Band, but for the demonstration of the prototypes, only the design at Ku-Band are fabricated and measured. For the dual-layer SIW power divider, the design is investigated at X-Band, Ku-Band and K-Band but fabrication and measurement are done at X-band only due to fabrication challenges on alignment and the existence of the air gap between substrate layers. The SIW coupler designed at Ku-band and has a wide bandwidth of about 31%. The SIW six-port without unused port is formed by single layer SIW power divider and SIW hybrid coupler, interconnected by delay transmission lines. It is successfully designed at the centre frequency of 14.5 GHz and has a bandwidth of about 20%. The dual-layer SIW power divider designed at 12 GHz and has high isolation of about 43 dB at 12.1 GHz. In the future work, the bandwidth of the SIW six-port can be improved by extending the length of SIW power divider transmission line and adding open circuit stub to improve the bandwidth of SIW power divider, consequently improve the bandwidth of the SIW six-port. The multilayer structure also has the potential to reduce the final dimension of the SIW six-port. For dual-layer structure, the research can be worked on SIW to slot-line transition to improve the isolation performance.

CHAPTER 1

INTRODUCTION

1.1 Research Background

The industrial environments are facing challenges so the increase in requirements making the traditional positioning sensors less desirable. The optical technique has the weakness in a harsh condition where the laser is hard to penetrate dust and fog which it is invented to be used under a clear condition (Bruder, et al., 2016) or direct contact (Amm, Simon, & Leung, 2017). The optical diffusion in a non-clear propagation media introduces measurement errors. Because of this disadvantage of the optical technique, the search for alternative measurement techniques is needed to bring a solution to this kind of conditions. One of the main alternatives for the optical technique is the radar technique. Throughout the innovation in the measurement technique, a radar principle based six-port interferometer have an excellent measurement properties providing solutions to several undesired effects (Engen, 1977). However, the classical six-port interferometer is large and bulky. This makes it irrelevant to be used as radar measurement in most of the industries.

Although the six-port technique has been invented for a few decades, but only being wildly implemented in the last decade in radar measurements (Francesco, Gabor, Stefan, Robert, & Alexander, 2012). The six-port DOA detector provides opportunities for innovations for novel industrial sensors and radar applications. Several six-port interferometer DOA technique have been developed and implemented for radar-based

sensor specific applications, such as traffic safety (Koelpin, A., Vinci, G., Laemmle, B., Lindner, S., Barbon, F., & Weigel, R., 2012), heart beat and respiration rate monitoring (Vinci, et al., 2013), or industrial vibration analysis (Mann, et al., 2013). These applications get benefit from the high accuracy low cost and low complexity of the Six-port interferometer.

Since the progress of the material technologies, the classical six-port interferometer can be transformed into PCB structure. As the progress of fabrication technology, the cost of PCB production is reduced. The reason of this phenomena is related to the progress in material technology and cheaper production cost of high-frequency planar electronic circuits (Hadi, Xu, Lin, Hui, & McKay, 2015). This introduced possibilities of implementing six-port interferometer in PCB. Since most of the component six-port technology can be built in high-frequency laminate boards as microstrip structures, this encourages the implementation of this technology in the industry.

The microstrip line has been used to design six-port with its low cost and small size advantages (Askari & Kamarei, 2017). The microstrip line is known best to be worked at low frequency but suffers from loss as the operating frequency increases (Zhu & Wu, 2002). Another better alternative designing technique for high frequency device is the Substrate Integrated Waveguide or known as SIW. The idea of integrated waveguide techniques was patented as early as 1995 (Piloto, Leahy, Flanick, & Zaki, 1995). Later in the year 1998, SIW was proposed and investigated theoretically and practically and proved to be able to be embedded in a substrate (Uchimura, Takenoshita, & Fujii, 1998). Similar to the microstrip line, SIW can be fabricated in

planar structure. SIW has a lower loss than microstrip as the operating frequency increases.

The operating mechanism of an SIW has similarities with conventional waveguide thus possess most of the advantages of conventional waveguide like high Q-factor and high power handling capability. SIW technique is a useful method and able to provide a solution in microwave communication system which gaining popularity among researchers (Vye, 2011). SIW have been used in the design of microwave components such as bandpass filter (Liu, Xiao, & Zhu, 2016), antenna (Caytan, et al., 2016) and coupler (Tavakoli & Mallahzadeh, 2018). There are also research on the miniaturization of the SIW components such as power divider (Khan & Mandal, 2016), bandpass filter (Xu, Ma, Meng, & Yeo, 2015) and antenna (Zhong, et al., 2017).

The SIW technology has already been researched for over one decade. Various of fields such as passive and active circuits, antennas and systems at microwave and millimeter-wave circuits have been researched including a various band of frequency from sub-gigahertz to sub-terahertz (Djerafi, Tarek, & Wu, 2013). Therefore, the development of six-port interferometer using SIW technique is an alternative in designing six-port, thus, providing innovation in designing low cost yet high-performance radar-based sensor.

1.2 Problem Statement

An SIW six-port was constructed using four SIW hybrid coupler (Lakhdhar, Harabi, & Gharsallah, 2015). Another SIW six-port was constructed using one SIW

power divider and three SIW hybrid coupler (Jafari, Moradi, Shirazi, & Mirzavand, 2017). However, those SIW six-ports have at least one extra port needed to be terminated. As a result, these design needed at least one more component for termination purpose. Therefore, an SIW six-port with no extra termination is a better design. Moreover, the SIW power divider used to construct the SIW six-port is low in isolation performance. This will have an effect on the six-port interferometer performance since the input signals might add up causing inaccuracy in the device.

There are a few designs on the SIW power divider with at least -10 dB isolation however the achievement of the isolation performance are obtained through a resistor chip (Yang, Chen, Lin, Yang, & Jin, 2016). The use of resistor component is a problem for the design with high frequency as it requires a specific size of the component to be able to mount in the circuit design. Therefore, an alternative technique in designing SIW power divider with high isolation is needed to provide innovation in PCB design.

1.3 The Objectives of The Study

The objectives of the research on the development of SIW six-port interferometer using Substrate Integrated Waveguide technique are as follows:

1. To design a new configuration of a SIW six-port with no unused ports, which has an operational bandwidth of 20% and better isolation performance without the use of resistor chip for high frequency radar-based application.

2. To analyze and validate the performance of the designed SIW power divider, SIW coupler and SIW six-port experimentally.

1.4 Research Scopes

To achieve the objectives, the scopes of the research are demonstrated as follows:

1. The SIW six-port structure without the unused port and its components such as power divider and hybrid couplers are designed at Ku-band (12-17 GHz) and K-Band (21-26 GHz) for radar-based application. All the designed are based on single layer structure. Only Ku-Band designs are fabricated and measured to validate the proposed single layer technique due to unavailable equipment for K-Band frequency range.

2. To improve the SIW six-port isolation performance without the use of resistor chip, dual-layer power divider is proposed to form the SIW six-port. The dual-layer power divider simulation is investigated over the frequency range of X-Band (9-12 GHz), Ku-Band (12-17 GHz). Because of the fabrication challenges of dual-layer structure at high frequencies (Ku-Band and K-Band), only the dual-layer power divider at X-Band is fabricated and validated experimentally. The SIW six-port structure formed by the dual layer power divider is not fabricated due to the fabrication difficulties.

3. The development of all the designs is designing using substrate RO4003C.

4. All of the designs are simulated using the CST microwave simulation tool.

1.5 Research Contribution

In these research work, SIW power dividers, SIW hybrid couplers and SIW six-ports are successfully designed.

The single layer SIW power divider designed at Ku-band has a wide bandwidth of about 20%. The SIW hybrid coupler designed at Ku-band using coupling aperture and modification of wider side wall technique successfully shows a wide bandwidth of about 30%. The designed SIW six-port at Ku-band shows the cascaded design of SIW power dividers and SIW couplers successfully form an SIW six-port without needed any external termination. The single layer SIW six-port designed at Ku-band has a bandwidth of about 20%.

The SIW six-port is also designed at K-band. The contraction of SIW six-port using the dual-layer SIW power divider is simulated at 24 GHz and the results show improved isolation performance in simulation. Therefore, the design can be used in the development of six-port interferometer providing innovation in designing high-performance radar-based sensor.

A new technique of design of dual-layer SIW power divider with improved isolation without using resistor is introduced. The SIW power divider is designed at X-band and shows high isolation performance of about 40 dB at 12 GHz.

1.6 Thesis Outline

The first chapter starts with some brief introduction of the positioning sensor technique of optical and radar, a six-port interferometer, PCB and SIW,. After that, the problem statement is defined for this research. The objectives are defined to overcome the problem statement. Research scopes are listed for this research. Finally, the research contribution in this research is stated.

In the second chapter, the radar-based sensor application is first introduced. After that, Six-port interferometer is elaborated. The SIW is elaborated with its structure and the formula regards the SIW and also the rules needed to be followed to design the SIW structure are shown. The transitions method between the microstrip line and SIW are also discussed. Literature review of the previous SIW power dividers, couplers and six-ports are elaborated and included in the chapter.

In the third chapter, the methodology of the design of the SIW six-port is presented. It starts with the project overview follow by the design specifications for the SIW power divider, SIW coupler and SIW six-port. The methodology of this research is shown in flowchart. The research of the SIW six-port begins with the design of the SIW power divider followed by the SIW coupler as the fundamental block before combined to perform SIW six-port. The simulation design software and process are discussed in the chapter. While the process of the fabrication is also discussed together with the fabrication prototypes followed by the measurement process as the final part of the chapter.

In chapter 4, the results of the SIW power divider, SIW coupler and SIW six-port are presented. The parametric study results are shown first for the dual-layer SIW power divider and SIW coupler designs. After that, the simulation results of the SIW power dividers, SIW couplers and SIW six-ports are presented. The fabricated SIW power dividers SIW coupler and SIW six-port measurement results are presented. Comparison between the simulation results and measurement results are done to verify the design. Discussion regards the errors occur are explained. Comparisons between the designs with the previous researches are also shown.

In chapter 5, the conclusion of the research on the SIW six-port presented. The summary regarding the SIW power divider, SIW coupler and SIW six-port are presented and the conclusion regarding the performance of the improved isolation for the dual-layer SIW power divider is specifically stated. The final part in this chapter carries the suggestions on possible future work to further explore the SIW power divider and SIW six-port.

CHAPTER 2

LITERATURE REVIEW

2.1 Introduction

This chapter contains five main sections and several subsections. First, the radar-based sensor application is introduced. After that, the six-port interferometer is elaborated. After the introduction of the six-port interferometer, SIW technology is presented. The literature review continues with the elaboration of the six-port main component with a review of the previous researched work in subsections of SIW power divider, SIW coupler and SIW six-port. Finally, this chapter is summarized up in the summary section.

2.2 Radar-based Sensor Application

The implementation of a laser interferometer (Jang, et al., 2016) as a positioning sensor in the industry is widely used due to its high accuracy, high resolution and excellent frequency response. The laser interferometer is built with optical high-resolution and non-contact distance measurement techniques. Although this technique requires no contact to operate it has its weakness. As shown in Figure 2.1, this optical technique depends on the optical lenses and mirrors to detect the objects and will suffer in harsh environments where it is difficult to penetrate dust and fog with the laser. Furthermore, the higher the density of suspended particle in the propagation environment the higher the dampening and scattering effects. As a result, the laser fails

to reach the surface of the object when the dampening and scattering effects too high. Because of the laser-based systems unable to operate in those conditions, the search for alternative measurement techniques without optical is necessary to be able to stand against such industrial environment conditions.

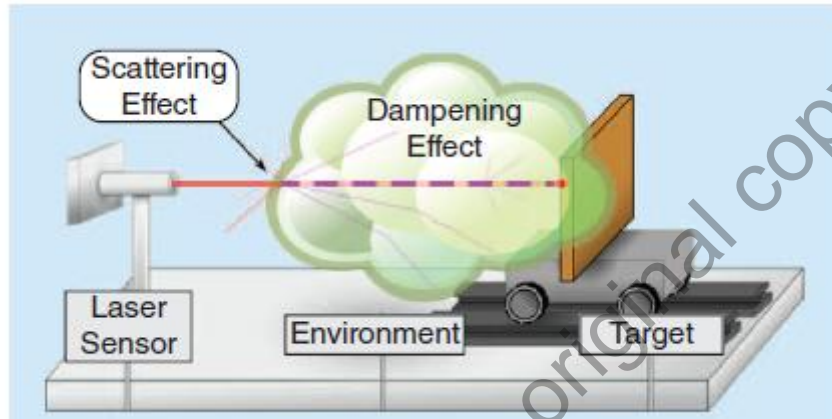


Figure 2.1 Optical technique detection in dusty environment (Vinci, Lindner, Barbon, Weigel, & Koelpin, 2012)

Radar technique is one of the most popular alternatives for non-contact based measurements (Pauli, et al., 2017). The concept of the radar technique is working through the propagation of microwave signals that can interact in a different medium as shown in Figure 2.2. Therefore, radar-based measurement techniques have the advantage over the optical measurement technique in harsh environments since radar waves do not encounter a problem when propagating through foggy or dusty air. Moreover, radar signal can even penetrate through bulky dielectric slabs or non-metallic shields whereas optical technique needed the dielectric slabs to be optically transparent.

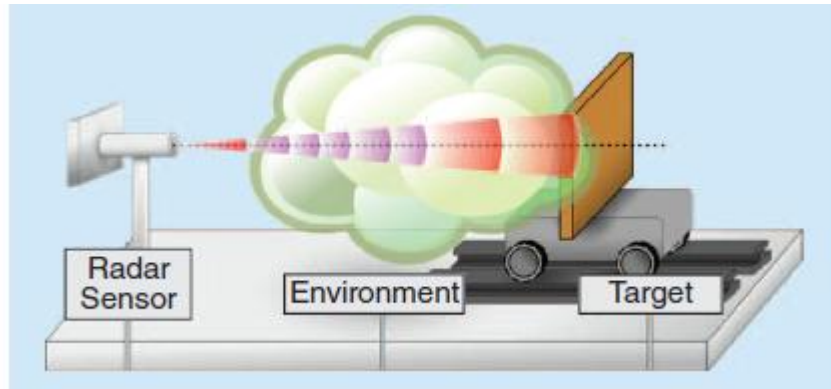


Figure 2.2 Radar technique detection in dusty environment (Vinci, Lindner, Barbon, Weigel, & Koelpin, 2012)

Within the last decade, radar technology has been rapidly expanding in industrial, automotive, and medical application areas. This is directly related to the advances developed in high frequency printed circuit board (Yu & Shi, 2015) and monolithic microwave integrated circuits (MMICs) (Sanders, et al., 2018) production. As a result, the manufacturing costs of microwave circuits have been reduced accordingly in the last decade. Therefore, radar is a cheaper measurement system compare to an equivalent optical measurement system.

Radar based sensor has been researched and can be use as a distance measurement system. The radar sensor has been used as automotive radar for safety and convenient purposes with the functions of adaptive cruise control (ACC) and autonomous emergency braking (AEB). There are also other radars such as multi-beam, multi-range radars (MBMR) which are formed by integration of narrow long range beam and wide short range beam as a single radar sensor (Lee, et al., 2017).

In industrial applications, radar is very useful as positioning sensors for automation process to track linear and rotational movements of various machinery. It is

important that less error occurs in the sensor interface to increase the accuracy of the positioning system as well as the quality of the overall automation process. The implementation of radar technology as positioning sensor performs the control systems and algorithms as an interface to the physical properties of the observed target and of the environment (Koelpin, et al., 2016).

In the medical applications aspects, the ability of radar technique in detecting human vital sign led to the application of earthquake rescue. The ability of microwave signal penetrate through debris after earthquakes make it possible to detect human activities where victims can't be search visually (Mabrouk, et al., 2016). Another important application is on the healthcare applications. Radar technique can provide the required high measurement accuracy to guarantee the safety of patients and the quality of therapies through vital sign monitoring systems (Wang, Tang, Chiu, & Horng, 2015). For example, the heartbeat and breath rate monitoring is done by detecting the tiny physiological movement without even needed to attach any sensor on the body (Liu, Gu, & Li, 2015).

The radar-based sensor can have its frequency ranges based on the frequency bands set by the International Telecommunications Union as shown in Table 2.1.

Table 2.1 Standard Radar-Frequency Letter-Band Nomenclature (International Telecommunication Union, 2016)

Band designation	Nominal frequency range	Specific frequency range for radar based on ITU assignments for Region 2
HF	3 MHz- 30 MHz	
VHF	30 MHz- 300 MHz	138 MHz- 144 MHz 216 MHz- 225 MHz
UHF	300 MHz- 1000 MHz	420 MHz- 450 MHz 890 MHz- 942 MHz
L	1000 MHz- 2000 MHz	1215 MHz- 1400 MHz
S	2000 MHz- 4000 MHz	2300 MHz- 2500 MHz 2700 MHz- 3700 MHz
C	4000 MHz- 8000 MHz	5250 MHz- 5925 MHz
X	8000 MHz- 12000 MHz	8500 MHz- 10,680 MHz
K	12 GHz- 18 GHz	13.4 GHz- 14 GHz 15.7 GHz- 17.7 GHz
K	18 GHz- 27 GHz	24.05 GHz- 24.25 GHz
Ka	27 GHz- 40 GHz	33.4 GHz- 36.0 GHz

2.3 Six-port Interferometer

The detection of the relative phase shift of the six-port receiver is based on DOA detection (Moghaddasi, Djerafi, & Wu, 2017) and the concept is illustrated in Figure 2.3. The six-port interferometer architecture is formed using one power divider, and three 90 degrees hybrid couplers with the label as P and H respectively. When the six-port work as a receiver, the operation of superposition of two input signals occur at four

outputs resulting in constructive or destructive interference. The six-port receiver also able to detect the relative phase shift between the two input signals.

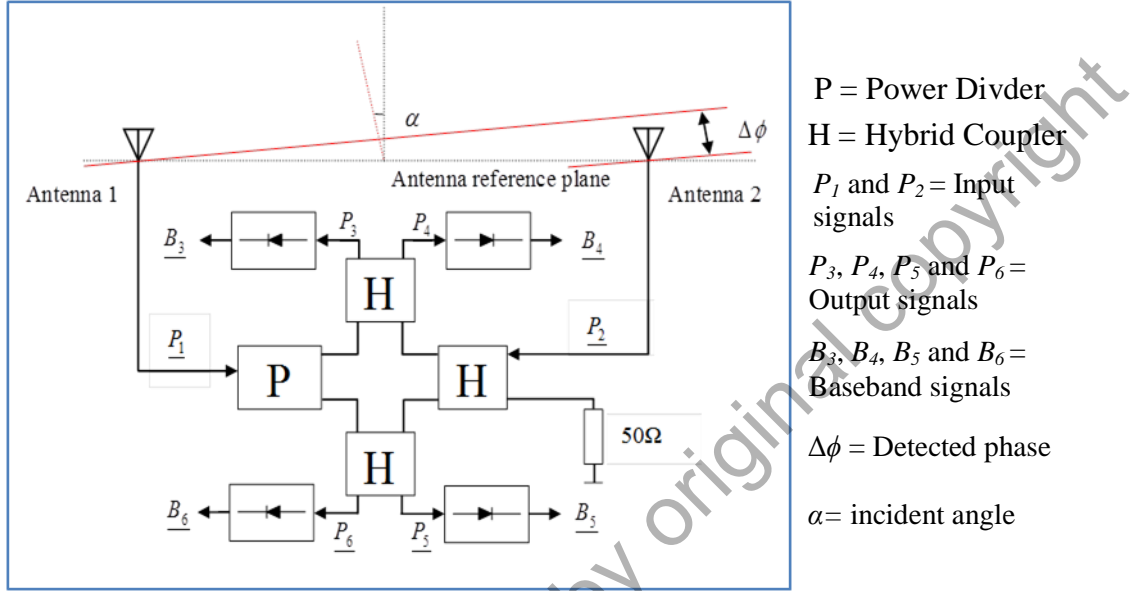


Figure 2.3 Six-port based DOA detection

By performing a phase difference measurement between the two receiving antennas aligned on a reference axis, the DOA angle of an incident wave with respect to the reference axis can be calculated. Two complex input signals P_1 and P_2 with carrier frequency f can be defined as (Vinci, et al., 2013):

$$\underline{P}_1 = A_1 e^{j(2\pi ft + \phi_1)} = A_1 [\cos(\omega t + \phi_1) + j \sin(\omega t + \phi_1)] \quad (2.1)$$

$$\underline{P}_2 = A_2 e^{j(2\pi ft + \phi_2)} = A_2 [\cos(\omega t + \phi_2) + j \sin(\omega t + \phi_2)] \quad (2.2)$$

with the radial frequency $\omega = 2\pi f$, the amplitude values A_1 and A_2 , the phase values ϕ_1 and ϕ_2 . Considering the relative quadrature phase differences between P_1 and

P_2 of $0, \pi/2, \pi$ and $3\pi/2$ RAD at the output ports, the complex output signals P_3, P_4, P_5 , and P_6 can be calculated as (Vinci, et al., 2013):

$$\underline{P}_3 = 0.5(\underline{P}_1 + j\underline{P}_2), \quad (2.3)$$

$$\underline{P}_4 = 0.5(j\underline{P}_1 + \underline{P}_2), \quad (2.4)$$

$$\underline{P}_5 = 0.5(j\underline{P}_1 + j\underline{P}_2), \quad (2.5)$$

$$\underline{P}_6 = 0.5(\underline{P}_1 - \underline{P}_2). \quad (2.6)$$

Down-conversion to baseband by power detectors delivers the following baseband voltages, $B_3 - B_6$ (Vinci, et al., 2013):

$$B_3 = |\underline{P}_3|^2 = 0.25|\underline{P}_1 + j\underline{P}_2|^2, \quad (2.7)$$

$$B_4 = |\underline{P}_4|^2 = 0.25|j\underline{P}_1 + \underline{P}_2|^2, \quad (2.8)$$

$$B_5 = |\underline{P}_5|^2 = 0.25|j\underline{P}_1 + j\underline{P}_2|^2, \quad (2.9)$$

$$B_6 = |\underline{P}_6|^2 = 0.25|\underline{P}_1 - \underline{P}_2|^2. \quad (2.10)$$

The baseband signals B_3, B_4, B_5 , and B_6 , can be handled like a differential I/Q signal (Vinci, et al., 2013):

$$I = \Re\{\underline{Z}\} = (B_5 - B_6), \quad (2.11)$$

$$Q = \Im\{\underline{Z}\} = (B_3 - B_4), \quad (2.12)$$

$$\underline{Z} = I + jQ + (B_5 - B_6) + j(B_3 - B_4) \quad (2.13)$$

Calculating the argument of the complex expression Z leads to (Vinci, et al., 2013):

$$\arg\{Z\} = \tan^{-1}\left(\frac{\Im\{Z\}}{\Re\{Z\}}\right) = \tan^{-1}\left(\frac{B_3 - B_4}{B_5 - B_6}\right). \quad (2.14)$$

The relationship between the incident angle, α and the detected DOA angle from the baseband signals, B_3 , B_4 , B_5 , and B_6 , of the six-port receiver, is therefore given by (Vinci, et al., 2013):

$$\alpha = \sin^{-1}\left[\tan^{-1}\left(\frac{B_3 - B_4}{B_5 - B_6}\right) \frac{\lambda}{2\pi L}\right] \quad (2.15)$$

Where λ is the wavelength of the signal and L is the distance between the two receiving antennas. The detected phase, $\Delta\phi$ is (Vinci, et al., 2013):

$$\Delta\phi = \tan^{-1}\left(\frac{B_3 - B_4}{B_5 - B_6}\right) \quad (2.16)$$

The detected angle accuracy will be optimized based on this formula.

2.4 Substrate Integrated Waveguide

SIW is a type of transmission line which can be fabricated in planar structure like CPW, microstrip and stripline. Since the mechanism of the SIW is about the same as a waveguide, it processes the ability of high power handling of the waveguide and the smaller size of able to be fabricated in planar structure. Thus, it is less bulky

compared to the conventional waveguide and has more power handling ability than others transmission lines such as CPW, microstrip and stripline.

2.4.1 SIW Structure

The structure of Substrate Integrated Waveguide has two rows of metallic via holes with certain gaps separating between the via holes and connecting the top and bottom planes of a dielectric substrate to form walls at each side of the dielectric substrate. The structure of the SIW is shown in Figure 2.4. The several parameters in the SIW are the diameter of the via holes d , the spacing between the via holes p , the width between the two periodic rows of metallic via holes w and thickness of the substrate h .

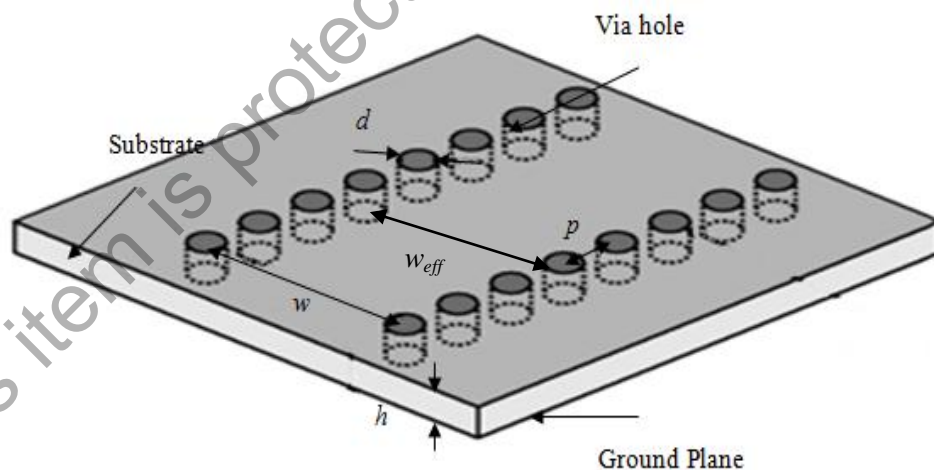


Figure 2.4 Structure of Substrate Integrated Waveguide (Xu & Wu, 2005)

The dispersion characteristics of SIW in a rectangular form is obtained by modeling using the BI-RME method combined with Floquet's theorem (Cassivi, et al., 2002). The analyzed results prove that both SIW and conventional rectangular

waveguide guided-wave characteristics are quite matching basically. Figure 2.5 shows the calculated results for the cutoff frequencies of the quasi- TE_{10} and quasi- TE_{20} modes of the SIW where pitch of the via holes b is fixed to 1.5mm.

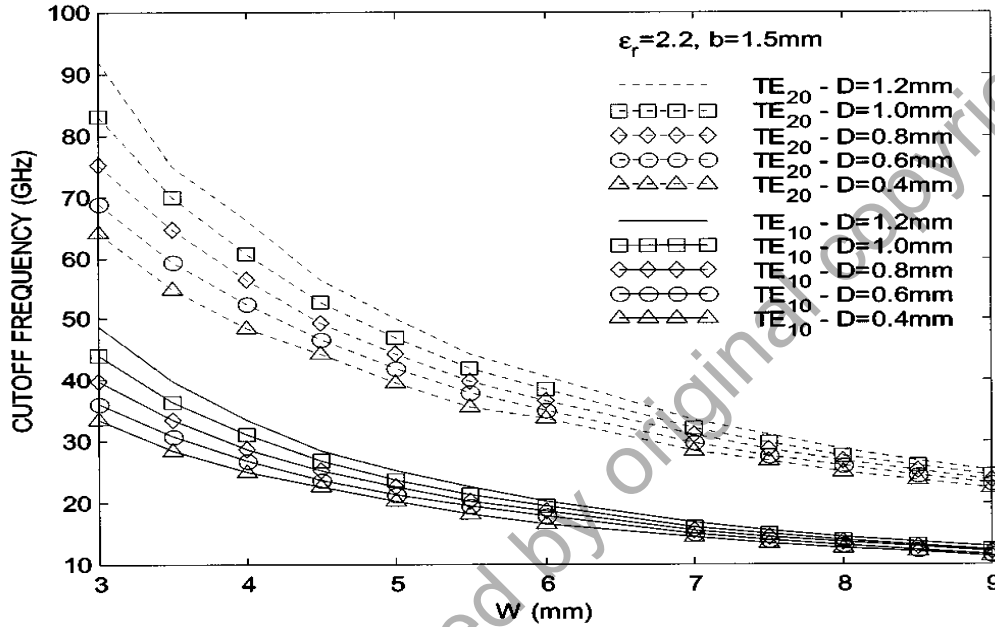


Figure 2.5 Cutoff frequencies of the TE_{10} -like and TE_{20} -like modes of the straight pattern SIRW vs. width W for various via diameters D (Cassivi et.al, 2002)

TE_{m0} modes are the modes that can exist in SIW structure. The derivation of the empirical equations for the first two dominant modes of the SIW are obtained from the calculated dispersion curves for cut-off frequency estimation and the equations are shown in (2.17) and (2.18) with the precision of (2.17) is within $\pm 5\%$ and the precision of (2.18) is possibly better than $+4\%/-9\%$. These approximations are valid for $p < \lambda_0 \cdot \sqrt{\epsilon_r} / 2$ and $p < 4d$. (Cassivi, et al., 2002).

$$f_{c(TE_{10})} = \frac{C_0}{2\sqrt{\epsilon_r}} \cdot \left(w - \frac{d^2}{0.95p} \right)^{-1} \quad (2.17)$$

$$f_{c(TE_{20})} = \frac{C_0}{\sqrt{\epsilon_r}} \left(w - \frac{d^2}{1.1p} - \frac{d^3}{6.6 \cdot p} \right)^{-1} \quad (2.18)$$

where C_0 is the speed of light in free space, λ_c is the cutoff wavelength and ϵ_r is the dielectric constant of the substrate.

As the dispersion characteristics for SIW in rectangular form are similar with the rectangular waveguide, the SIW can be analyzed as a rectangular waveguide by equalling the width as the effective width of the SIW represented as w_{eff} . The equation can be derived from (2.17) as (2.19) with the condition of the spacing between the metallic via holes is sufficiently small (Cassivi, et al., 2002).

$$w_{eff} = w - \frac{d^2}{0.95 \cdot p} \quad (2.19)$$

Leakage loss occurs between each metallic via holes, therefore the gaps, p between each metallic via holes must be kept small, however, the loss also occurs at the via hole diameter, d . Research done on the SIW filter has discovered that the ratio of d/p has much more influence than the pitch of the via holes because both of the parameters are interrelated. The mechanism of SIW using periodic rows of metallic via holes to form the wall is unlike the normal homogeneous waveguide. Therefore, the via hole diameter has a significant impact on the return loss of the waveguide section because of its input port. Two design rules related to the via holes diameter and the pitch of the holes have been formulated as (2.20) and (2.21) to be followed to achieve negligible radiation loss in SIW where λ_g is the guided wavelength (Wu, Deslandes, & Cassivi, 2003).

$$d < \frac{\lambda_g}{5} \quad (2.20)$$

$$p \leq 2d \quad (2.21)$$

The region of SIW to have equivalent leakage losses and bandgap as the conventional waveguide in its operating bandwidth is defined in (2.22) and (2.23) (Deslandes & Wu, 2006). The condition of (2.22) is to make sure that the circuit is physically realizable and the condition of (2.23) is to prevent any bandgap occurred where λ_c is the cutoff wavelength.

$$p > d \quad (2.22)$$

$$\frac{p}{\lambda_c} < 0.25 \quad (2.23)$$

SIW technology is able to be fabricated in planar form to form a complete circuit using any planar processing techniques on a standard printed circuit board (Djerafi, Tarek, & Wu, 2013). Besides, chip-sets mounting on the same substrate is also possible. Transition losses are reduced since no components fabricated other than planar processing technologies. These properties allow the concept of System-in-Package (SiP) which is widely adopted in the design of RF circuits, applicable to the System-on-Substrate. System-on-substrate represents the ideal platform for developing cost-effective, easy-to-fabricate and high-performance mm-wave systems.

The characteristic of the SIW in planar design proves that it is one of the types of substrate integrated circuits. Therefore, SIW components not only have the advantages of planar printed circuits but also metallic waveguides. These make SIW be

able to use as a substitute for microstrip and coplanar lines with the advantages of light, easy to fabricate, compact, cost-effective and flexible but also possess advantages of the conventional waveguide of low loss, high quality-factor and complete shielding. These make SIW better in terms of Q-factor and power handling than traditional planar microstrip or stripline.

2.4.2 Microstrip to SIW Transition

The structure of SIW is different compared to microstrip line. Therefore, transition is needed in order to interconnect different structures. A good transition design can bring strong impacts to the performance of the system. There are various types of the transition section can be used for realization. One of those is coplanar waveguide (CPW) to SIW transition (Nwajana, Dainkeh, & Yeo, 2017) which has been used in the SIW bandpass filter design. Another type is Ground coplanar waveguide (GCPW) to SIW transition which has been used in the research of SIW slot antenna (Li & Li, 2019). Another different type of transition is used in the design of ridged SIW magic-T which is the stripline to SIW transition (Wang & Ling, 2019). The most popular type of transition is the microstrip line to SIW transition which have further modification in the design (Askarian & Moradi, 2016).

Although microstrip line and waveguide are two different structures, the electric fields of both structures are approximately oriented in the same direction. So, they are well suited and share the same profile. The dominant mode of electric profiles for rectangular waveguide and microstrip line are shown in Figure 2.6.

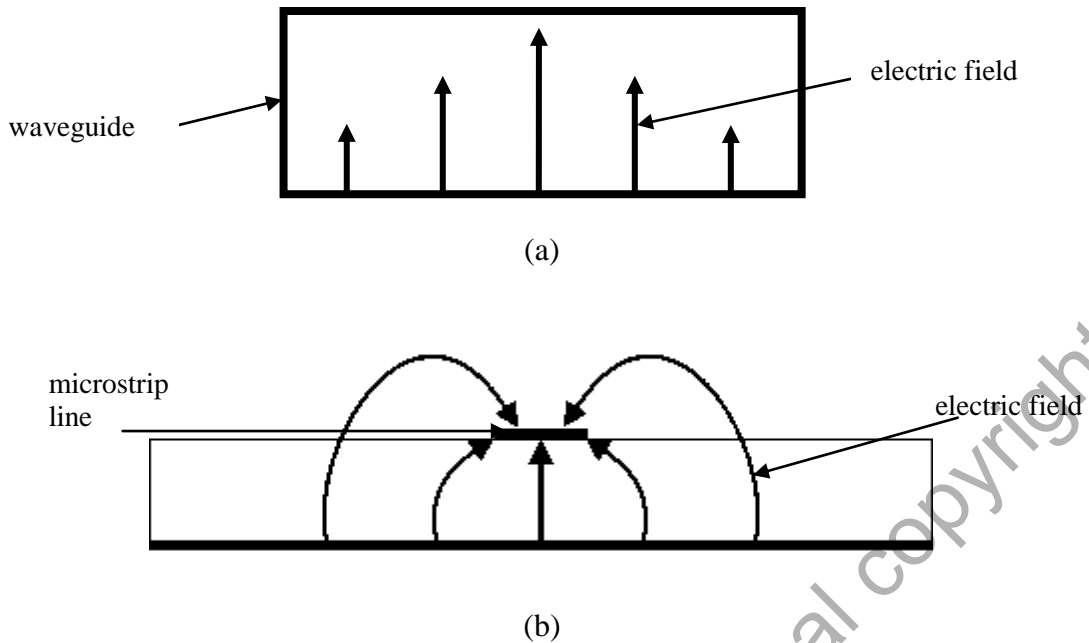


Figure 2.6 Dominant mode electric profiles: (a) rectangular waveguide; (b) microstrip line (Pozar, 2005)

A microstrip line integrates with SIW in planar platform via a simple taper (Caleffo, 2016); (Dousset, Wu, & Claude, 2010); (Keltouma, Mohammed, & Saghir, 2011) has been proposed and good results had been obtained with good effective bandwidth, high return loss and low insertion loss. As the substrate thickness increases the radiation loss also increases during the transition and strong coupling to the nearby integrated circuit may occur. Further, analyze needed to be done on the circuits together with the transition using electromagnetic modeling package in order to have a more accurate prediction of the entire structure response.

The transition of microstrip to SIW through taper design is shown in Figure 2.7. The taper transition provides matching by converting the quasi- TEM mode propagating in microstrip line into the quasi- TE_{10} mode in rectangular waveguide. The realization of the side walls of the SIW can be done by either using arrays of metalized grooves, metallic via-posts, paste side walls or other techniques.

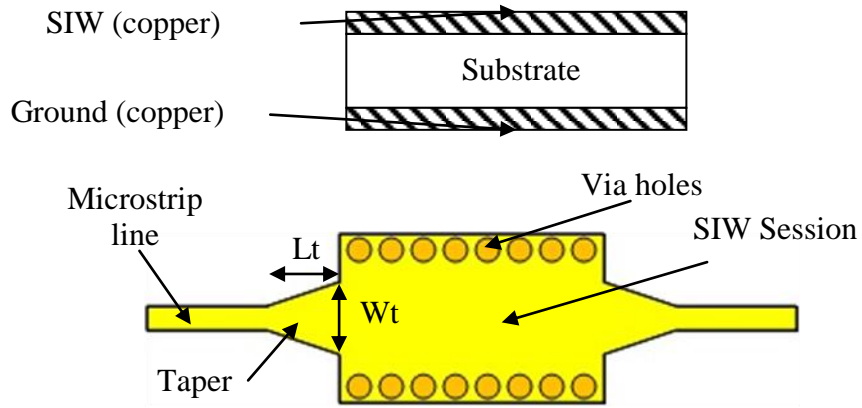


Figure 2.7 Taper transition of microstrip line to SIW

Taper width (W_t) and taper length (L_t) are parameters for microstrip taper design. These parameters can be determined by the equations as shown in (2.24), (2.25), (2.26) (Bozzi, Georgiadis, & Wu, 2011); (Doghri, Djerafi, Ghiotto, & Wu, 2015); (Kumar, Jadhav, & Ranade, 2012):

$$W_t = w + 0.1547W_{eff} \quad (2.24)$$

$$L_t = 0.2368\lambda_{g-ms} \quad (2.25)$$

$$\lambda_{g-ms} = \frac{\lambda_{g0}}{\sqrt{\epsilon_{reff}}} \quad (2.26)$$

where W_{eff} is the width of SIW. λ_{g-ms} is the guided wavelength of the microstrip line, λ_{g0} is the wavelength in free space and ϵ_{reff} is the effective permittivity which can be determined using Equation (2.30) and w is the width of the microstrip transmission line can be determined using equation (2.27), (2.28) and (2.29)

$$\frac{w}{h} \left\{ \begin{array}{l} \frac{8e^A}{e^{2A}-2} \quad \text{for } \frac{w}{h} < 2 \\ \frac{2}{\pi} \left[B-1 - \ln(2B-1) + \frac{\epsilon_r-1}{2\epsilon_r} \left\{ \ln(B-1) + 0.39 - \frac{0.61}{\epsilon_r} \right\} \right] \quad \text{for } \frac{w}{h} > 2 \end{array} \right\} \quad (2.27)$$

$$A = \frac{Z_0}{60} \sqrt{\frac{\epsilon_r+1}{2}} + \frac{\epsilon_r-1}{\epsilon_r+1} \left(0.23 + \frac{0.11}{\epsilon_r} \right) \quad (2.28)$$

$$B = \frac{377\pi}{2Z_0\sqrt{\epsilon_r}} \quad (2.29)$$

$$\epsilon_{r\text{eff}} = \frac{\epsilon_r+1}{2} \left(1 - \frac{1}{2h} \left(\frac{\epsilon_r-1}{\epsilon_r+1} \right) \left(\ln\left(\frac{\pi}{2}\right) + \frac{1}{\epsilon_r} \ln\left(\frac{4}{\pi}\right) \right) \right) \quad (2.30)$$

where Z_0 is the characteristic impedance of the microstrip line and h is the thickness of the substrate (Kumar, Jadhav, & Ranade, 2012).

2.5 Six-port Main Components

The six-port is a passive circuit, can be constructed in different ways with components such as hybrid couplers, power dividers and phase shifters. The structure of six-port consists of two inputs and four outputs. One input is for the unknown signal and the other for the reference signal while four outputs are the linear combinations of two input signals. Since the SIW six-port could be constructed by either combination from power divider and coupler, the literature review is not only limited to SIW six-port but also on SIW power divider and SIW coupler.

2.5.1 SIW Power Divider

Power divider is a passive microwave component with the function of power division or power combining. The power division can be an input signal divided into